minerals

MDPI

Article

Effect of the Sodium Silicate Modulus and Slag Content on Fresh and Hardened Properties of Alkali-Activated Fly Ash/Slag

Xiaowei Ouyang [1], Yuwei Ma [1,2,*], Ziyang Liu [1], Jianjun Liang [1] and Guang Ye [3]

[1] Guangzhou University-Tamkang University Joint Research Center for Engineering Structure Disaster Prevention and Control, Guangzhou University, Guangzhou 510006, China; xwouyang@gzhu.edu.cn (X.O.); 2111816164@e.gzhu.edu.cn (Z.L.); 2111916101@e.gzhu.edu.cn (J.L.)

[2] Centre for Future Materials, University of Southern Queensland, West Street, Toowoomba, QLD 4350, Australia

[3] Department of Materials and Environment (Microlab), Faculty of Civil Engineering and Geosciences, Delft University of Technology, 2628CN Delft, The Netherlands; G.Ye@tudelft.nl

* Correspondence: yuwei_ma@gzhu.edu.cn or yuwei.ma@usq.edu.au; Tel.: +86-020-39366432

Received: 8 November 2019; Accepted: 18 December 2019; Published: 23 December 2019

Abstract: This paper presents the results of an experimental study performed to investigate the effect of activator modulus (SiO_2/Na_2O) and slag addition on the fresh and hardened properties of alkali-activated fly ash/slag (AAFS) pastes. Four activator moduli (SiO_2/Na_2O), i.e., 0.0, 1.0, 1.5, and 2.0, and five slag-to-binder ratios, i.e., 0, 0.3, 0.5, 0.7, 1.0, were used to prepare AAFS mixtures. The setting time, flowability, heat evolution, compressive strength, microstructure, and reaction products of AAFS pastes were studied. The results showed that the activator modulus and slag content had a combined effect on the setting behavior and workability of AAFS mixtures. Both the activator modulus and slag content affected the types of reaction products formed in AAFS. The coexistence of N–A–S–H gel and C–A–S–H gel was identified in AAFS activated with high pH but low SiO_2 content (low modulus). C–A–S–H gel had a higher space-filling ability than N–A–S–H gel. Thus, AAFS with higher slag content had a finer pore structure and higher heat release (degree of reaction), corresponding to a higher compressive strength. The dissolution of slag was more pronounced when NaOH (modulus of 0.0) was applied as the activator. The use of Na_2SiO_3 as activator significantly refined the pores in AAFS by incorporating soluble Si in the activator, while further increasing the modulus from 1.5 to 2.0 prohibited the reaction process of AAFS, resulting in a lower heat release, coarser pore structure, and reduced compressive strength. Therefore, in view of the strength and microstructure, the optimum modulus is 1.5.

Keywords: alkali-activated fly ash/slag; activator modulus; slag content; fresh and hardened properties

1. Introduction

In recent years, as cement production is facing challenges of CO_2 emission and a shortage of raw materials, alkali-activated materials (AAMs) or geopolymers are attracting increasing attention as an alternative binder to ordinary Portland cement (OPC) [1,2]. AAMs are developed via alkaline activating of the solid aluminosilicates, such as fly ash, blast furnace slag, and mine tailings, at a high pH. The reaction process consists of dissolution of the raw materials and polymerization of the dissolved ions in a high alkaline solution, such as sodium hydroxide or sodium silicate solutions. In alkali-activated low calcium system, for example, Class F fly ash as the raw material, the reaction product is a three-dimensional tetrahedral framework of SiO_4 and AlO_4 linked by shared oxygen as siloxo (–Si–O–Si–O–), sialate (–Si–O–Al–O–), sialate–siloxo (–Si–O–Al–O–Si–O–), and sialate–disiloxo

(–Si–O–Al–O–Si–O–Si–O–), with alkali metal ions (e.g., Na^+) balancing the charge associate with tetrahedral Al [3]. This type of gel is known as N–A–S–H gel. In an alkali-activated high calcium system, for example, blast furnace slag as the raw material, the reaction product is a two-dimensional calcium silicate hydrate with a certain degree of Al-participation, also known as C–A–S–H gel. In an alkali-activated fly ash/slag (AAFS) blended system, the main reaction product is a coexistence of N–A–S–H gel and C–A–S–H [4]. AAMs can not only provide comparable performance to OPC [5] but also reduce CO_2 emissions [6] and solid wastes [7,8]. Moreover, AAMs have advantages of rapid setting and hardening [9], high compressive strength [10–12], high durability [13,14], low thermal conductivity, high fire resistance [15], resistance to alkali aggregate reaction [16], and high freeze-thaw resistance [17].

Although there are many advantages of the AAMs, the application of these materials has some limitations so far. In general, AAMs are sensitive to the type of raw materials (low-calcium or high-calcium system), as well as the modulus and concentration of the alkali activator [18]. As mentioned above, AAMs activated by different raw materials may result in different types of reaction products (N–A–S–H, C–A–S–H, or coexistence of both). Different products possess varied properties: N–A–S–H gel is reported to exhibit high chemical resistance, fire resistance, and good durability, mainly due to its three-dimensional tetrahedral framework. C–A–S–H gel is similar to the reaction product of OPC, i.e., C–S–H gel, which presents a higher space filling effect than the N–A–S–H gel and leads to a much denser microstructure than OPC. Lloyd et al. [19] found that adding a certain proportion of blast furnace slag in the fly ash system can significantly reduce the porosity of the system. Compared with the alkali activated slag system, the addition of fly ash can reduce the shrinkage and inhibit the development of cracks. The chemical constitution of alkali activator and its concentration are also found to have significant effects on the strength development and the reaction kinetics of AAMs [20,21]. Palomo et al. [22] pointed out that compared with the NaOH-activated system, the water glass activator contains a large number of soluble silicates. The presence of soluble Si in water glass promotes the formation of gel. Phoo-ngernkham et al. [23] reported that the polymerization process of AAMs could be enhanced by using sodium hydroxide together with sodium silicate rather than using sodium hydroxide alone. The Na_2O/SiO_2 modulus was also found to have an important effect on the microstructure and mechanical properties of geopolymers [24,25]. Wu et al. [26] reported that the high pH activators could accelerate the reaction process of AAMs. Ravikumar and Neithalath [20] studied the influence of the activator alkalinity on the mechanical properties and microstructures of AAMs. The results showed that a higher alkalinity led to a higher compressive strength of AAMs.

The raw material and activator concentration had a significant effect on the reaction products, reaction kinetics, and engineering properties of AAMs. In addition, the reaction process of alkali-activated slag/fly ash system is more complex than that of alkali-activated slag or fly ash system. There is no consensus among the types of reaction products of the alkali-activated fly ash/slag blended system yet, while the combination effect of raw material and activator modulus on the reaction process of AAFS is still not clear. It is reported by Provis et al. [27] that C–(A)–S–H gels were the dominate reaction products when the slag content was 25% and 50%, where samples with 25% or lower slag contents were dominated by N–A–S–(H) gels. Ismal et al. [28] found that in a blended system with more than 50% of fly ash, a hybrid type gel described as N–(C)–A–S–H was identified since part of the Ca released by slag dissolution is incorporated into the N–A–S–H type gel. To this end, in the present paper, AAFS was investigated in terms of different fly ash/slag content and different activator modulus. The combined effect of activator modulus and fly ash/slag content on setting time, flowability, heat evolution, compressive strength, microstructure, and reaction products of an alkali-activated fly ash/slag blended system were systematically studied.

2. Materials and Methods

2.1. Materials

Ground granulated blast furnace slag and class F fly ash were used in this study. The chemical composition of the fly ash and slag is given in Table 1. The amorphous content in the fly ash, measured by the chemical dissolution method (EN 196), was 58.6%. The specific surface area of the granulated blast furnace slag and class F fly ash were 485 and 290 m^2/kg, respectively. The particle size distribution (PSD) of fly ash and slag is shown in Figure 1. The crystalline phases in the fly ash and slag were analyzed by X-ray diffraction (XRD), and the XRD spectrum is shown in Figure 2. It shows that the major crystalline phases in fly ash are mullite ($3Al_2O_32SiO_2$) and quartz (SiO_2). Akermanite ($Ca_2MgSi_2O_7$) is the major crystalline phase in the slag. The morphology of the fly ash and slag is shown in Figure 3. Fly ash particles are spherical, and the slag particles are more lozenge shaped.

Table 1. Chemical compositions of fly ash and slag.

Oxide	SiO_2	Al_2O_3	Fe_2O_3	CaO	MgO	Na_2O	K_2O	LOI*
Fly ash (wt %)	49.1	34.8	4.5	4.9	0.4	0.4	1.3	2.3
Slag (wt %)	32.6	16.4	0.4	38.7	7.1	0.3	0.3	0.5

LOI* = Loss on Ignition.

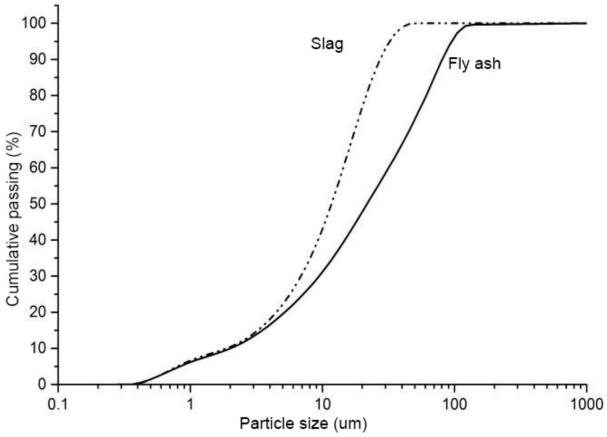

Figure 1. Particle size distribution of fly ash and slag.

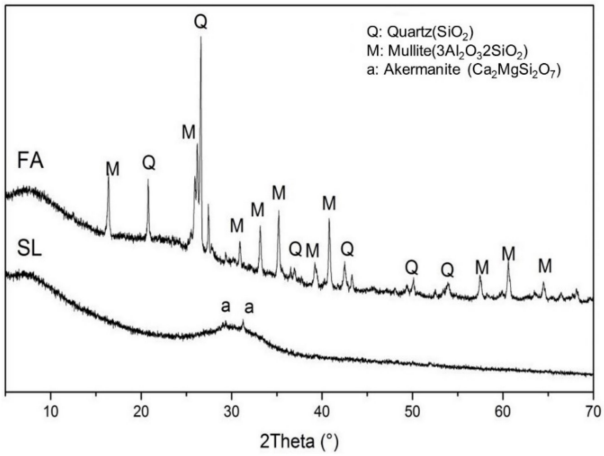

Figure 2. X-ray diffraction analysis of the fly ash and the slag.

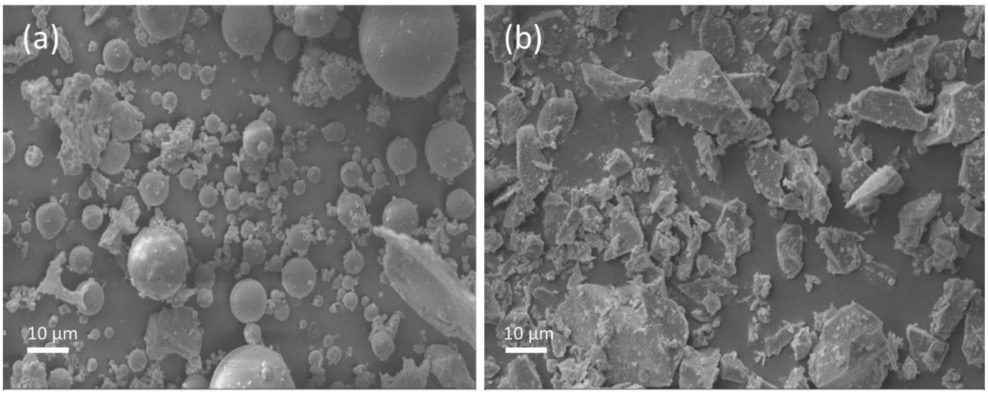

Figure 3. Morphology of the fly ash (**a**) and the slag (**b**).

The alkali activators were prepared by mixing sodium hydroxide (99% purity) with distilled water and a sodium silicate solution ($Na_2O{\cdot}nSiO_2{\cdot}mH_2O$, SiO_2/Na_2O = 2.16, water content = 61.5 wt %, specific gravity 1.38 g/mL). The alkali activator was prepared as follows: NaOH solution was prepared first, and the sodium silicate solution was then mixed with the NaOH solution to form an alkali activator. The prepared activator was left overnight to cool down to room temperature. In order to investigate the effect of the sodium silicate activator modulus on fresh and hardened properties of alkali-activated fly ash/slag paste, a series of activating solutions with different SiO_2/Na_2O modules, i.e., 0.0, 1.0, 1.5, 2.0, were prepared. The binders were prepared by dry mixing of slag and fly ash with five different slag to binder ratios, i.e., slag/binder = 0.0, 0.3, 0.5, 0.7, and 1.0. The mix proportion of the samples is listed in Table 2. In order to identify the different mixtures easily, mixtures are denoted by their substitution level of slag (S) and activator modulus (N). For example, S7N10 corresponds to the mixture containing 70% slag with an activator modulus of 1.0. The binder was premixed for 1 min, the alkali activator was then added, and the paste was mixed for a further 4 min. Fresh pastes were cast into molds (40 mm cube), consolidated, sealed, and cured under atmospheric pressure at 20 °C for 24 h.

Table 2. Mix composition of fly ash/slag geopolymer pastes.

Name	Fly Ash (g)	Slag (g)	The Activator Modulus (SiO_2/Na_2O)	SiO_2 (g)	Na_2O (g)	Water (g)
S0N0	100	0	0	0	4.89	35
S3N0	70	30	0	0	4.89	35
S5N0	50	50	0	0	4.89	35
S7N0	30	70	0	0	4.89	35
S10N0	0	100	0	0	4.89	35
S0N10	100	0	1.0	5.90	6.10	35
S3N10	70	30	1.0	5.90	6.10	35
S5N10	50	50	1.0	5.90	6.10	35
S7N10	30	70	1.0	5.90	6.10	35
S10N10	0	100	1.0	5.90	6.10	35
S0N15	100	0	1.5	7.11	4.89	35
S3N15	70	30	1.5	7.11	4.89	35
S5N15	50	50	1.5	7.11	4.89	35
S7N15	30	70	1.5	7.11	4.89	35
S10N15	0	100	1.5	7.11	4.89	35
S0N20	100	0	2.0	7.91	4.09	35
S3N20	70	30	2.0	7.91	4.09	35
S5N20	50	50	2.0	7.91	4.09	35
S7N20	30	70	2.0	7.91	4.09	35
S10N20	0	100	2.0	7.91	4.09	35

2.2. Methods

2.2.1. Setting Time

The setting time of the paste is an important parameter since it shows the time available for effective handling of the paste. In this study, the Vicat needle method based on the ASTM C191 standard [29] was used to determine the setting time. The fresh pastes were immediately poured into a truncated cone mold to measure the setting time at room temperature. The initial setting time is defined as the time between the initial contact of the binder with the activating solution and that when the distance between the needle and the base-plate was 6 ± 3 mm. The final setting time corresponds to the point when the needle first penetrated only 0.5 mm into the specimen [29].

2.2.2. Workability

The mini-slump spread test was used to determine the workability of the pastes. Firstly, the fresh pastes were filled into the mold. After 15 s, the mold was lifted vertically. After another 30 s, the diameters of the paste spread were measured along two perpendicular directions. The average diameter was interpreted as the workability of the pastes.

2.2.3. Heat of Hydration

The rate of heat evolution of all the mixtures was measured by an isothermal conduction calorimeter (TAM-Air-314, TA Instruments Ltd., New Castle, NE, USA). Prior to the experiment, the calorimeter was calibrated at 20 °C, and the materials (fly ash and slag) were stored at 20 °C for 24 h. In the testing procedure, fly ash and slag powder was first mixed with the alkali solution for 1 min, and then a 10 ± 0.01 g paste sample was carefully poured into a glass ampoule and transferred into the calorimeter channel. The whole procedure lasted for about 3 min. The heat flow was recorded, and the cumulative heat was calculated up to 168 h.

2.2.4. Compressive Strength

The mixtures were prepared in a Hobart mixer according to the standard procedure described in ASTM C305 [30]. The paste samples were poured into cube molds of 40 × 40 × 40 mm^3. Afterward, plastic foils were used to seal the surfaces of specimens to avoid moisture losses. Then, the specimens were stored in the laboratory at 20 ± 2 °C for 1 day. After demolding them, the specimens were kept in the standard curing chamber with a constant temperature of 20 ± 2 °C and a relative humidity of 95 ± 5% until the designated testing age. Compressive strength was tested at 7 and 28 days. The average values of three samples were interpreted as the compressive strength of the pastes for each age.

2.2.5. Porosity, SEM/EDS Analysis

The samples were crushed into small pieces and kept in a mixture of alcohol and acetone (1:1 *v*/*v*, respectively) for one week to stop the reaction process. Then, the samples were taken out of the solution and dried in an oven at 60 °C under vacuum. The pore structure of the samples was analyzed by MIP (AutoPore IV9500, Micromeritics Instrument Ltd., Norcross, GA, USA). Detailed information on the experimental method can be found in [31]. The morphology and elemental analysis of the hydration products were determined by means of the SEM/EDS technique (Hitachi TM3030, Hitachi High-Technologies Ltd., Kagoshima, Japan).

3. Results and Discussion

3.1. Setting Time

Figure 4 shows the effect of the activator modulus and slag content on the initial setting time and final setting time of AAFS pastes. As observed, the initial setting time presented different trends as the activator modulus and slag content varied. For the fly ash/slag blended system, the initial setting

time varied between 20 to 50 min, which is quite short compared to that of OPC. This is in agreement with previous findings [32]. In general, the initial setting time and final setting time decreased when the activator modulus increased from 0.0 to 1.5, and then increased at 2.0. It is reported that the early reaction of AAFS is a diffusion-controlled process. The setting behavior of AAFS is closely related to the presence of Ca in pore solution [33]. In the alkaline liquid environment with Ca present, the raw materials immediately begin to dissolve after contacting with the activator, releasing elements such as Ca, Al, and Si ions. Unlike NaOH as the activator, the sodium silicate with the modulus of 1.0, 1.5, and 2.0 already had a large amount of active Si at the beginning of the reaction, so the dissolved Ca and Al elements can quickly combine with Si to form the gel. It led to a decrease in the final setting time. However, the continuous increase of modulus led to a lower pH of the activator. High silica concentration in the solution is only useful through the presence of a large amount of silanol groups in the solution. Further increase of Si content reduces the amount of monomeric silica, which is needed to help with the hydrolysis reaction [7]. Therefore, the setting time increased when the modulus increased to 2.0. A different trend was shown for the pure fly ash system, for which the initial setting time increased as the modulus increased from 0.0 to 1.5, and then suddenly decreased at 2.0. It indicated a different reaction mechanism affecting the setting behavior of the alkali-activated fly ash system.

The effect of the slag content on setting time of AAFS pastes is also shown in Figure 4. It can be seen that the initial and final setting time decreased for AAFS with higher slag content when the modulus of the activator was 0, 1.0, and 1.5. For AAFS with an activator modulus of 2.0, both the initial setting time and final setting time increased as the slag content increased. Due to the low reactivity of fly ash, AAFS mixtures with higher fly ash content (less slag content) had longer setting time. This is in line with the findings from previous research [34]. The addition of slag with higher reactivity than fly ash promotes the dissolution of raw materials in the early stage and increases the content of elements such as Ca and Al in the liquid phase of the system, resulting in shorter initial and final setting time of AAFS. However, a different trend was found when the activator modulus was 2.0. It indicates that a combined effect existed as the raw material and activator modulus varied. The use of higher modulus as the activator prohibited the initial dissolution of slag, leading to a longer setting. It is observed that the setting time was the shortest for alkali-activated fly ash with silica modulus 2.0. An increase of silica concentration led to a higher degree of silicate ion polymerization in the alkali solutions [35]. For a higher amount of silica, the fraction of monomer and dimer form of the silicate species decreased, while the fraction of trimer units grew [36]. The monomeric and dimeric silicates reacted with the aluminate anions that dissolved from fly ash, forming an initial aluminosilicate gel, and reorganization of the gel continued to form a gel with high polymerization, while silicate trimers that existed in high silica solution could directly react with the aluminate anions for form aluminosilicate gel with relatively high polymerization. Thus, a shorter setting time was observed for alkali-activated fly ash with silica modulus 2.0.

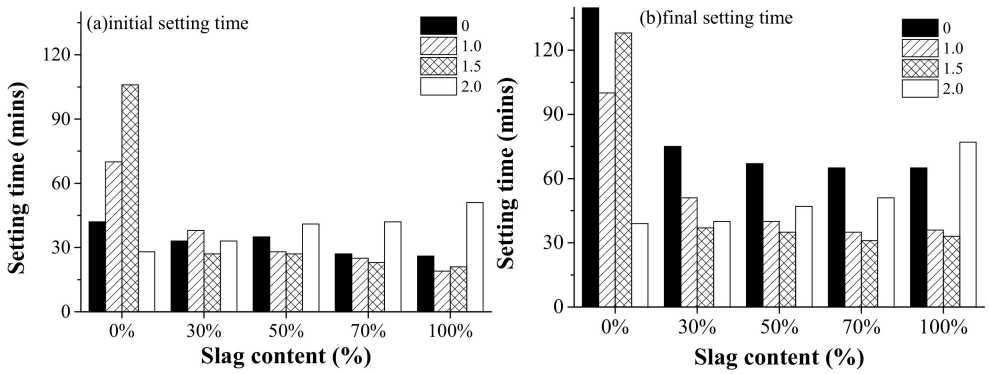

Figure 4. The effect of the activator modulus (0, 1.0, 1.5, 2.0) and the slag content (0%, 30%, 50%, 70%, and 100%) on (**a**) the initial setting time and (**b**) final setting time of alkali-activated fly ash/slag (AAFS) pastes.

3.2. Flowability

The results of the mini-slump spread tests are shown in Figure 5. In general, the value of the spread diameter was higher for AAFS with an activator modulus of 1.0 and 1.5, while the use of an activator modulus of 0.0 and 2.0 resulted in reduced workability. Previous research [37] has reported that the activator has an essential effect on the rheological performance of the AAFS pastes. It has been proved that the rheology depends on the modulus of sodium silicate for AAFS pastes. AAFS mixtures with the largest spread diameter and the shortest final setting were recorded at the modulus of 1.5. It is possible that a large amount of active [SiO_2] at the beginning of the reaction can capture the dissolved Ca and Al elements, which can lead to strong adhesion forces between binder particles [38–44].

The effect of the slag content on the flowability of the AAFS pastes was also shown in Figure 5. The effect of slag content on flowability varied for AAFS mixtures with a different activator modulus. When the activator was 1.0 and 1.5, the flowability did not change significantly as the slag content varied. When the activator modulus was 0.0, the flowability slightly decreased as the slag content increased, while the trend was the opposite when the slag content was 2.0. As we know, fly ash was able to enhance the workability in the fresh OPC system due to its spherical shape [45]. Thus, the workability was expected to decrease as the fly ash content decreased in AAFS. This is the case for the AAFS mixture activated by NaOH (activator modulus of 0.0). It is possible that the use of water glass had a more significant effect on the flowability than the fly ash/slag content. Therefore, the flowability exhibited a different trend when the activator modulus was 1.0, 1.5, and 2.0.

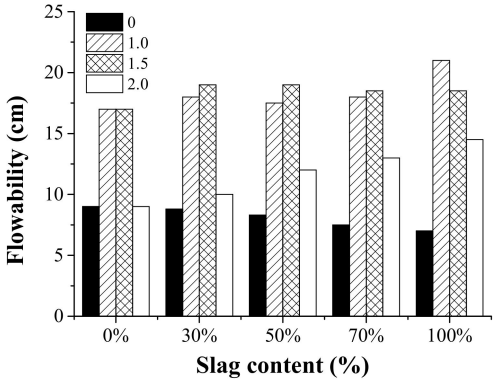

Figure 5. The effect of the activator modulus (0, 1.0, 1.5, 2.0) and the slag content (0%, 30%, 50%, 70%, and 100%) on the spread diameter (flowability) of the AAFS pastes.

3.3. Heat Evolution of AAFS Pastes

The effect of the activator modulus and slag content on the heat evolution and cumulative heat of the AAFS pastes is shown in Figures 6 and 7. As can be seen from Figure 6, only one exothermic peak appeared for the alkali-activated pure fly ash system, while two exothermic peaks were observed in the AAFS blended system and alkali-activated slag system. It is reported that the first exothermic peak was related to the initial wetting and dissolution of raw materials in the first stage [46]. With the increase of slag content, the additional exothermic peak occurred. The second peak appeared between 5 h and 50 h, which was related to the formation of more reaction products. An increase of slag content can accelerate the reaction process of the AAFS paste, and the second peak appeared in a shorter time and with higher intensity. For the AAFS blended system and alkali-activated slag system, the appearance of the exothermic peak was delayed for AAFS with a higher activator modulus. The heat evolution results indicated that the higher activator modulus prohibited the formation of reaction products, leading to a lower degree of reaction. The occurrence of two heat release peaks in this study was in agreement with the heat evolution of alkali activated fly ash/slag in previous studies [47,48]. The lower the modulus, the higher the pH of the liquid phase of the system. The higher pH caused a higher degree of fly ash and slag dissolution of the AAFS system and, therefore, a higher degree of reaction.

Figure 7 presents the accumulative heat of AAFS pastes with different activator moduli and different slag content. It appears that an increase of the activator modulus resulted in a lower heat release. For alkali-activated fly ash activated by NaOH (activator modulus of 0.0), the accumulative heat was lower than the sodium silicate activated mixtures, while for the blended system activated by NaOH, the accumulative heat became higher than the Na_2SiO_3-activated mixtures as the slag content increased. This means that the use of sodium silicate as the activator promoted the reaction in the pure fly ash system while it hindered the reaction in the fly ash/slag blended system. By using the acid attack method, Criado et al. also found a lower degree of reaction for mixture with a higher silicate content [24]. The use of water glass was able to provide soluble Si to the geopolymer reaction. In the alkali-activated fly ash system, Al dissolved faster than Si in the raw material. Al could react with the soluble Si in the activator to form reaction products. Therefore, the degree of reaction is higher when the modulus increased from 0 to 1.0. In the fly ash/slag blended system, the pH of the activator seems to have a dominant effect on the dissolution of slag. The dissolution of slag was more pronounced when NaOH was used as the activator. AAFS pastes with higher slag content had a higher cumulative heat release at 7 days, indicating a higher degree of reaction.

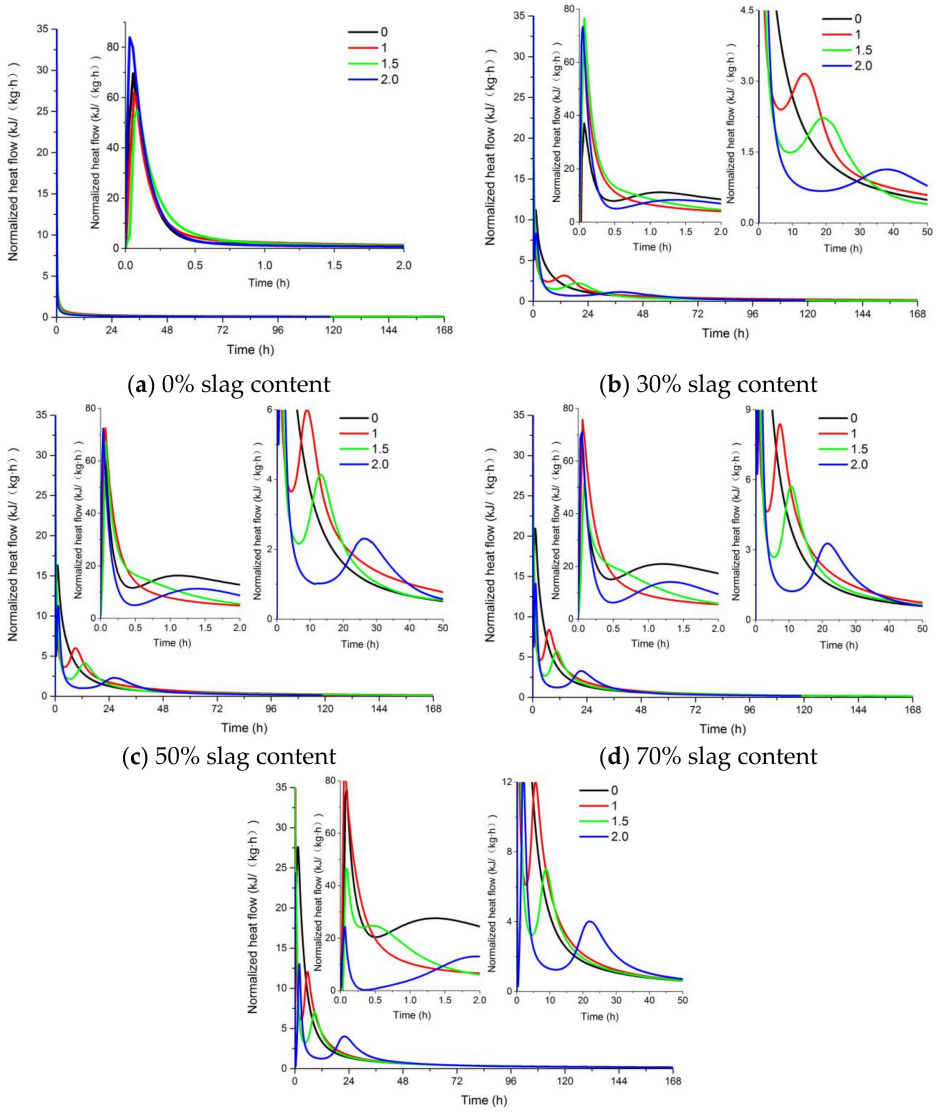

(**a**) 0% slag content (**b**) 30% slag content

(**c**) 50% slag content (**d**) 70% slag content

(**e**) 100% slag content

Figure 6. The effect of the activator modulus and slag content on the heat evolution of AAFS. (**a**) 0% slag content; (**b**) 30% slag content; (**c**) 50% slag content; (**d**) 70% slag content; (**e**) 100% slag content.

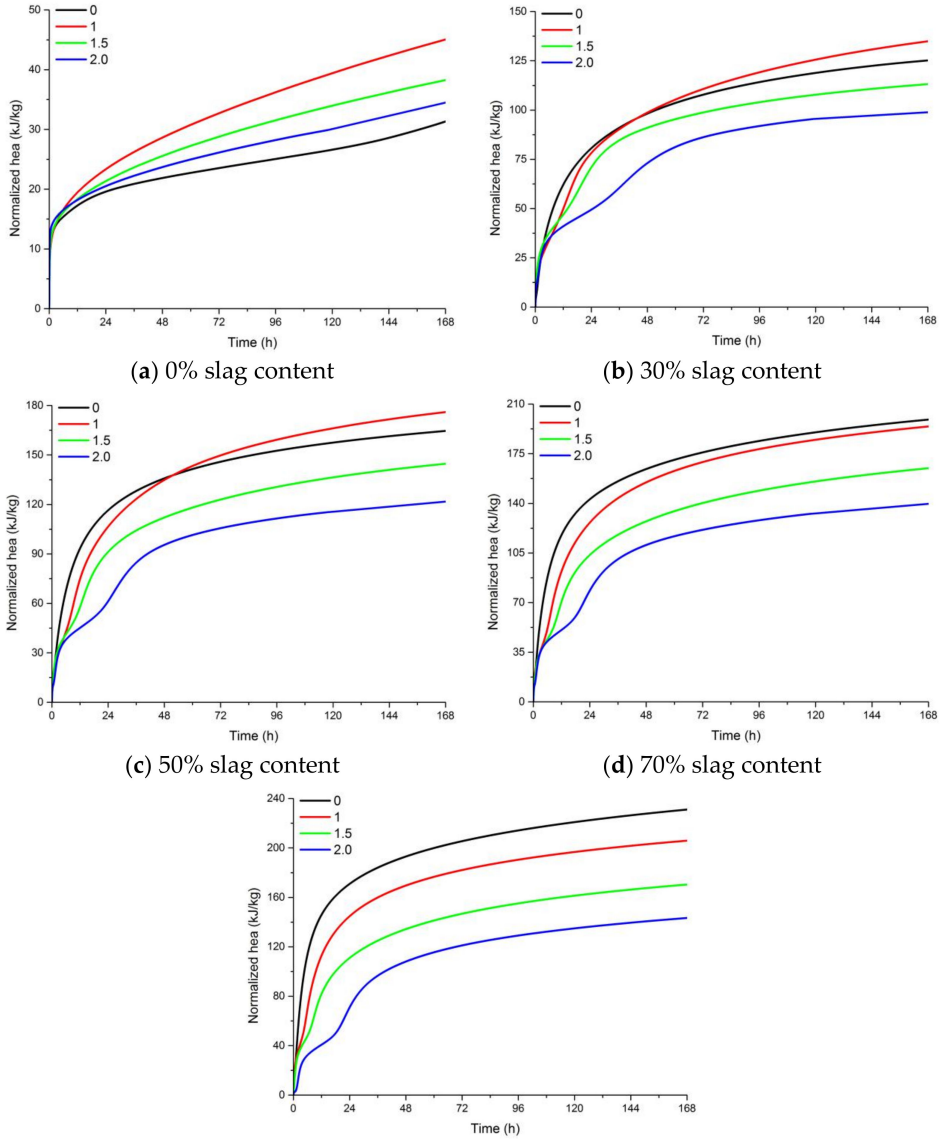

(**a**) 0% slag content (**b**) 30% slag content

(**c**) 50% slag content (**d**) 70% slag content

(**e**) 100% slag content

Figure 7. The effect of the activator modulus and slag content on the cumulative heat release of AAFS. (**a**) 0% slag content; (**b**) 30% slag content; (**c**) 50% slag content; (**d**) 70% slag content; (**e**) 100% slag content.

3.4. Compressive Strength

Figure 8 shows the effect of the activator modulus and the slag content on compressive strength at the curing age of 7 and 28 days. As can be seen, the compressive strength at 7 days generally decreased as the activator modulus increased from 1.0 to 2.0. This is consistent with the cumulative heat release results, as shown in Figure 7, that AAFS mixtures with a higher activator modulus presented lower cumulative heat release at the curing age of 7 days. At the age of 28 days, the AAFS mixture with an activator modulus of 1.5 exhibited the highest compressive strength. The use of only NaOH as activator significantly decreased the compressive strength compared to the use of sodium silicate. By using ^{29}Si NMR, Li et al. [32] reported that as the activator modulus increased, the monomer (Q_0) and dimmer (Q_1) silicon groups decreased while trimer (Q_2) and octamer (Q_3) units increased. This is related to the formation of less negatively charged Si–O^- groups due to the decrease in pH of the activator. The alkali activator reaction was known to be enhanced for activator with more monomer and dimmer silicon groups. When the modulus increased from 0 to 1.0, although the Na_2O in modulus

1.0 was higher, the added [SiO_2] decreased the pH of the activator. Therefore, we observed that the cumulative heat release of modulus 0.0 was first lower and then became higher than that of modulus 1.0 as the slag content increased. That means the dissolution of slag may be more pronounced in the NaOH system. This is supported by a previous study indicating that the dissolution of slag was more extensive in high pH [32]. On the other hand, the added [SiO_2] was able to react with the dissolved Ca, Al, and Si from the raw materials, forming the reaction products, leading to a denser microstructure. More fly ash and slag particles were dissolved, leading to a higher degree of reaction. When the alkali content in the activator increased from 1.0 to 2.0, the excessive [SiO_2] decreased the pH of the activator and prohibited further dissolution of the raw material particles, leading to a lower degree of reaction. It resulted in the reduction of the compressive strength. Therefore, a too low or too high activator modulus is unfavorable for the development of the strength.

The effect of the slag content on the compressive strength is also shown in Figure 8. It can be seen that the compressive strength at both 7 days and 28 days increased with increasing slag content. When the slag content was 100%, the compressive strength was the highest. With increasing slag content, the amount of active Ca increased. It can promote the reaction of the system, produce C–A–S–H gel substances [27], and improve the strength of the system. Compared with the effect of the activator modulus, the effect of slag content on compressive strength was much stronger.

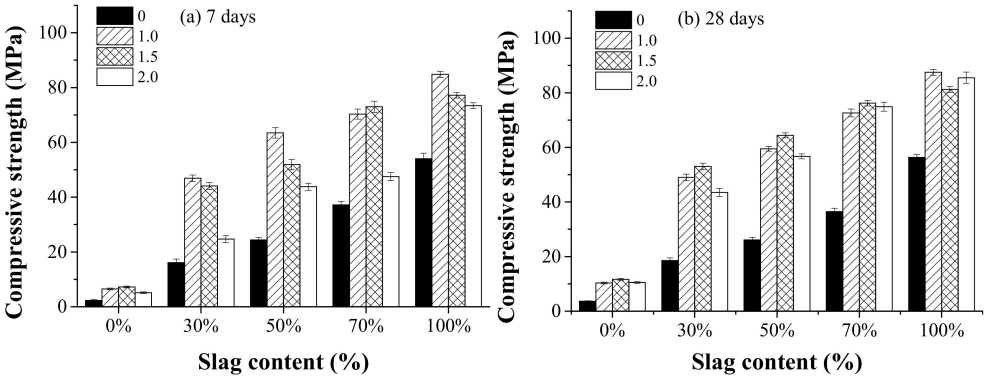

Figure 8. The effect of the activator modulus (0, 1.0, 1.5, 2.0) and the slag content (0%, 30%, 50%, 70% and 100%) on compressive strength at the curing age of 7 days (**a**) and 28 days (**b**).

Table 3 compares the compressive strength derived from this study with references. Phoo-ngernkham [23] prepared AAFS with low-calcium fly ash and GBFS (fly ash/GBFS = 1), and sodium silicate solution with a modulus of 2.56 was applied as the activator. The obtained strength at 7 days was 84.9 MPa, much higher than the strength obtained in this study (Table 3). In this study, a further increase the modulus to 2.0 resulted in a lower strength. It is likely that the overall NaOH content in the activator was much higher in the reference than this study. For economic reasons, the Na_2O/(fly ash/slag) ratio was kept lower than 6.1%. The use of slag with low calcium content in AAM resulted in a considerably lower compressive strength (10.8 MPa at 7 d and 14 MPa at 28 d) [49]. Heat curing (80 °C) and sodium silicates as the activator could increase the compressive strength of the low calcium slag system [50]. Fly ash with high calcium content was found to exhibit high strength after heat curing [4]. That indicated the importance of calcium in the strength development of the alkali-activated reaction. Soultanan et al. [18] mixed metallurgical slag with brick waste (calcium resource) and obtained AAM with a relatively high compressive strength (48.9 MPa) after heat curing. However, the use of high content of slag also has other issues such as high autogenous and drying shrinkage. In most situations, the use of slag exceeding 70% is not recommended. Otherwise, there is a high risk of cracking in AAFS [46,51].

Table 3. Comparison of compressive strength of alkali-activated materials with references.

Raw Materials	SiO_2/Na_2O Ratio	Temperature (°C)	Curing Age (Days)	Compressive Strength (MPa)	Reference
Low-calcium slag and kaolin (69:9)	3.4	60	7	10.8	[49]
High-calcium fly ash	4.8	60	2	62.6	[4]
Brick waste and metallurgical slag (1:1)	1.16	90	7	48.9	[18]
Fly ash and GBFS (1:1)	2.56	23	7	84.9	[23]
This study (FA/SL = 1:1)	1.5	20	7	52	-

3.5. Porosity and Pore Size Distribution

In order to investigate the microstructure of AAFS, some representative AAFS mixtures were chosen for analysis. Figure 9a,b depicts the pore structure and total porosity of the AAFS paste (with slag content of 30%) with the activator modulus of 0, 1.0, 1.5, 2.0 at the curing age of 7 days, respectively. As can be seen, the modulus had a great effect on the pore size distribution and total porosity. The AAFS paste with the modulus of 0 had the highest total porosity, and most of the pores were capillary pores with diameters in the range of 0.01 to 0.1 μm. The use of water glass as the activator could significantly refine the pore structure of AAFS. AAFS with the activator modulus of 1.0 exhibited the lowest total porosity and lowest critical pore diameter at 4 nm. A further increase of the activator modulus from 1.0 to 2.0 resulted in a higher total porosity and coarser critical pore diameter (Figure 9a). Such results were consistent with both the cumulative heat release and compressive strength results. As mentioned in Section 3.4, excessive $[SiO_2]$ in the activator with higher modulus decreased the pH of the activator and prohibited further dissolution of the raw material, which are unfavorable for the development of the microstructure.

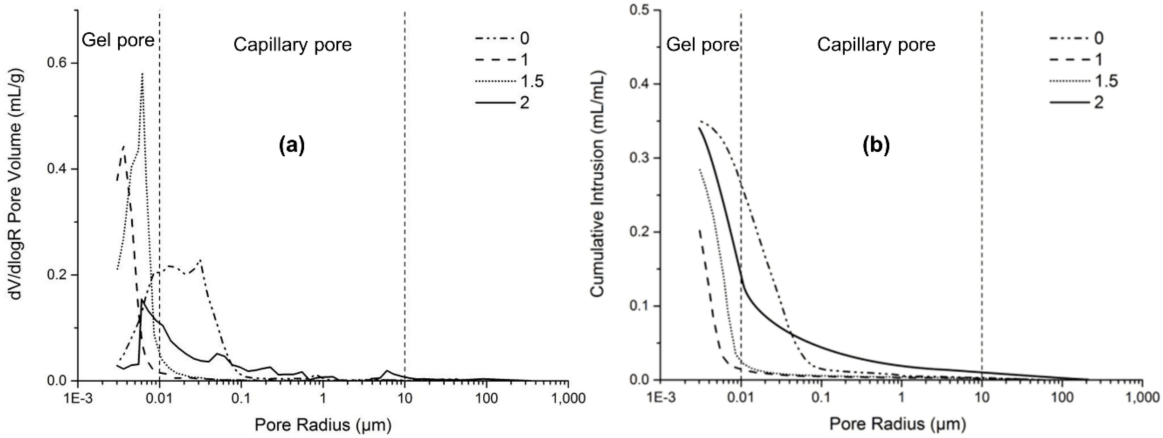

Figure 9. The pore structure (**a**) and total porosity (**b**) of the AAFS paste with different activator modulus (the slag content is 30 wt. %) at the age of 7 days.

Figure 10 presents typical MIP results of AAFS pastes with different slag content (activator modulus of 1.5). Alkali-activated fly ash exhibited considerably larger pore size distribution than the fly ash/slag blended system. The critical pore size of pure fly ash system was at around 0.15 μm, most of which belonged to capillary pores. With the increase of slag content, the total porosity decreased, and the pore structure became smaller. The critical pore size decreased from 8 to 3 nm, around two orders of magnitude lower than the pure fly ash system. Fewer capillary pores can be found in the fly ash/slag blended system; almost all of the pores belonged to the gel pores. It indicates that the blending of slag greatly decreased the capillary pores and increased the gel pores in the system, leading to lower total porosity and smaller pores.

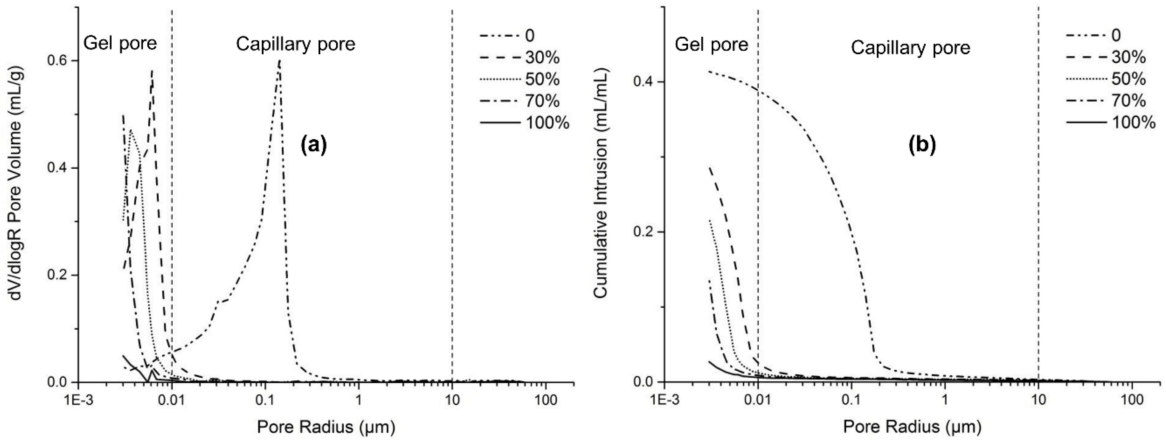

Figure 10. The pore structure (**a**) and the porosity (**b**) of the AAFS paste with different slag content (the activator modulus is 1.5) at the age of 7 days.

3.6. SEM Analysis

Figure 11 shows typical SE images of the AAFS pastes with the different moduli at the curing age of 7 days (the slag content is 30%). As can be seen from Figure 11a, when the modulus was 0, the reaction products were loosely consolidated, and the sample was porous. A small number of needle-like reaction products can be observed. This was in line with the MIP results that pure fly ash system had the most porous microstructure. Accordingly, the corresponding compressive strength of the sample was only 16.1 MPa at 7 days. When the modulus increased to 1.0 and 1.5, it seems that the overall structure became denser and more homogenous, and the corresponding compressive strength of samples with the modulus of 1.0 and 1.5 was 46.9 MPa and 44.1 MPa, respectively. When the modulus increased to 2.0, the microstructure was less homogenous (Figure 11d), and more unreacted fly ash/slag particles existed in the matrix. Accordingly, the compressive strength of AAFS with activator modulus 2.0 decreased to 24.7 MPa at 7 days. Compared with the AAFS paste with a modulus of 0, the overall structure of the paste with the modulus of 2.0 is denser, so its compressive strength is higher. The results indicate that the modulus determines the structure and morphology of the reaction products.

Figure 12 presents the typical microstructure of the AAFS pastes with different slag content at 7 days (the activator modulus is 1.5). As can be seen from Figure 12a, there are many unreacted fly ash particles in the alkali activated pure fly ash system. Few reaction products were observed, and it was hard to form a steady skeleton and develop compressive strength. Therefore, the compressive strength of the pure fly ash system was very low. When the slag content increased to 30% (Figure 12b), the microstructure became much homogenous, but small pores and unreacted fly ash particles were still observed. With the increase of the slag content to 50%, less pores were found, and the microstructure became denser. The SEM results are inconsistent with the results of the MIP test, as shown in Figure 10. When the slag content increased to 70% (Figure 12d) and 100% (Figure 12e), the fly ash particles in the system were almost completely reacted. AAFS with 70% slag presented a homogenous microstructure, while the alkali-activated slag system exhibited significant cracks in Figure 12e. These cracks were caused by the drying procedure during the SEM measurements, which also indicated that alkali-activated slag (or with high content of slag) were prone to cracking under dry conditions.

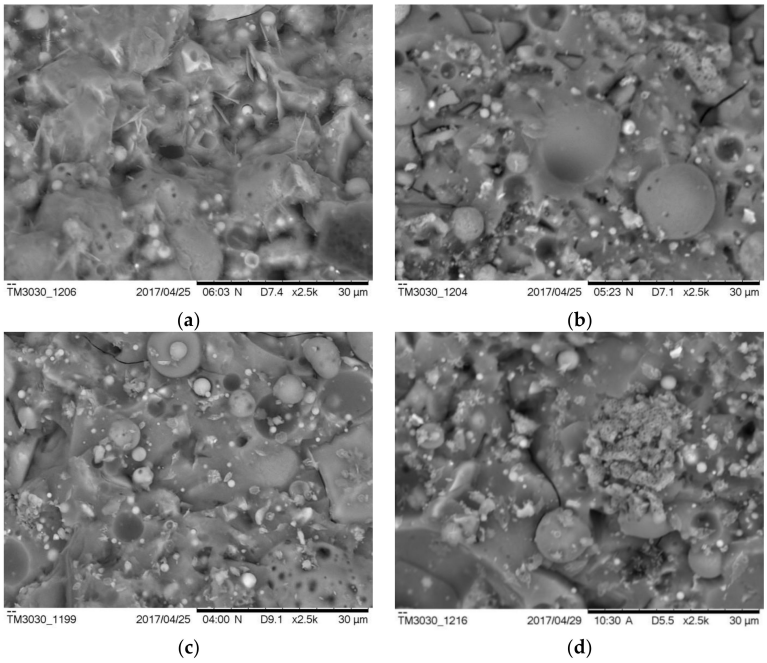

Figure 11. The microstructure of the AAFS pastes with the activator modulus of 0 (**a**), 1.0 (**b**), 1.5 (**c**), and 2.0 (**d**) at 7 days (the slag content is 30 wt %).

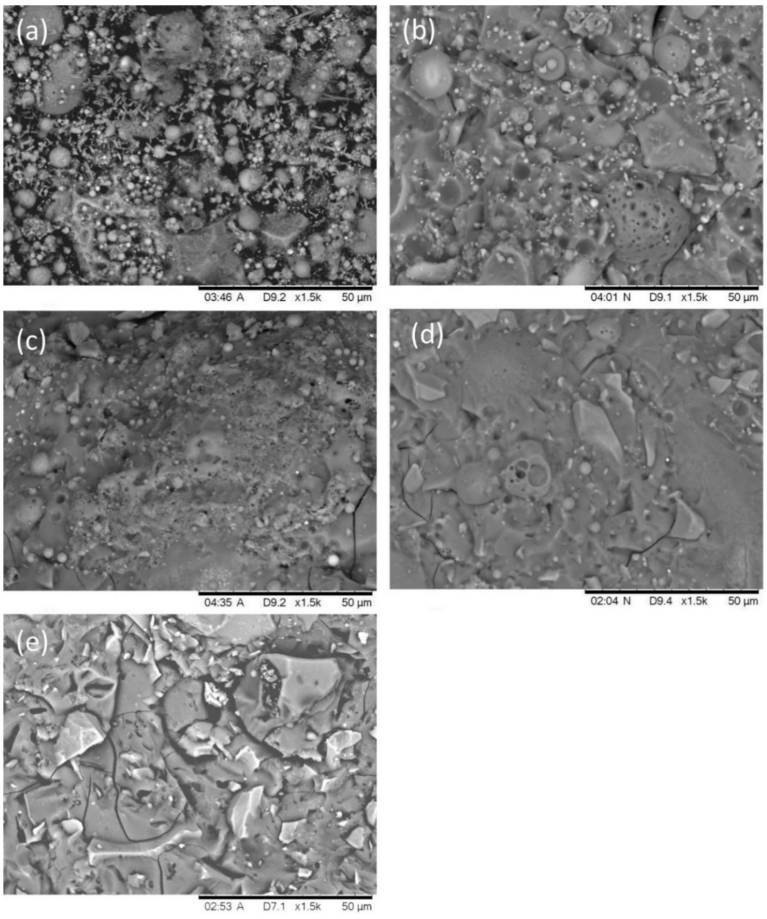

Figure 12. The microstructure of the AAFS with the slag content of 0 (**a**), 30% (**b**), 50% (**c**), 70% (**d**), and 100% (**e**) at 7 days (the activator modulus is 1.5).

3.7. EDS Analysis

Figure 13a shows the typical elementary composition of the AAFS pastes with different activator moduli (the slag content is 30%). As mentioned above, two types of gel may exist in the alkali-activated fly ash/slag blended system: a class of three-dimensional tetrahedral frameworks of SiO_4 and AlO_4, also known as N–A–S–H gel [28] and a two–dimensional calcium silicate hydrate with certain degree of Al–participation, known as C–A–S–H gel [28]. There is still no consensus among the types of reaction products formed in the AAFS system as the raw material and activator modulus varied. As shown in Figure 13, for the AAFS paste system with the activator modulus of 0 and 1.0, two different types of gels were clearly identified: N–A–S–H type gel with a low Ca content and a high amount of Al content, and C–A–S–H type gel with a high Ca content and a lower amount of Al. However, when the activator modulus increased to 1.5 or 2.0, the reaction products of the AAFS became homogeneous, with a higher Si content in the reaction products. Such results were seldom reported in previous studies. It is known that the activator with a modulus of 0 and 1.0 had higher pH and less soluble Si. It is likely that fly ash and slag particles dissolved faster in this condition, and the reaction products precipitated around the raw materials. Therefore, two types of gels were formed in these two systems. As the activator modulus increased to 1.5 and 2.0, the pH of the activator decreased, and more soluble Si was present in the system, which led to a lower dissolution of fly ash and slag particles. Meanwhile, soluble Si participated in the geopolymerization reaction, forming a more homogenous reaction product. The results obtained here indicated that a higher activator modulus within the system not only changed the dissolution of the vitreous structure of the binder particles but also affected the types of the reaction products in the AAFS blended system.

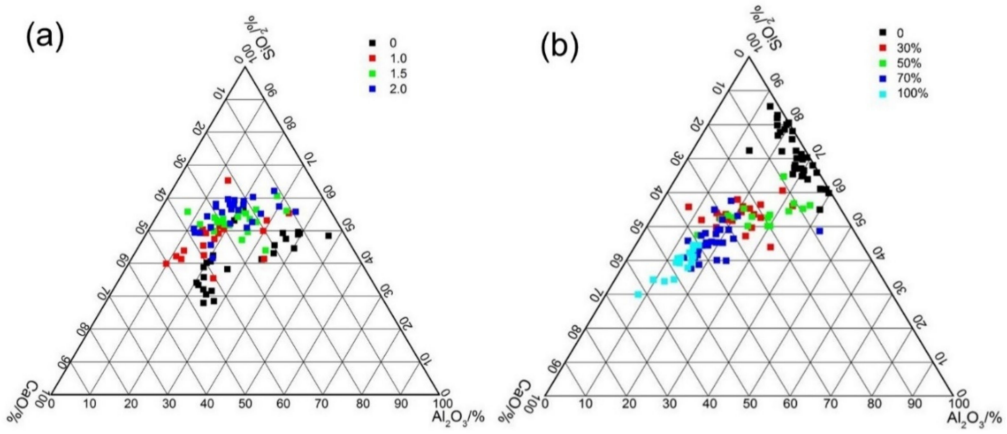

Figure 13. Al_2O_3–SiO_2–CaO ternary representations of EDS data of the AAFS paste with different activator modulus (the slag content is 30 wt %) (**a**) and that with different slag content (the activator modulus is 1.5) (**b**) at 7d.

Figure 13b shows the typical elementary composition of the AAFS pastes with different slag content (the activator content is 1.5). In the pure fly ash system, the reaction products are a class of N–A–S–H. As the slag content increased, the gel gradually changed from N–A–S–H gel to C–A–S–H gel. This is in line with the findings from a previous study [35]. Compared with the pore structure results as discussed in Figure 10, it can be concluded that the C–A–S–H gel had higher space filling ability than the N–A–S–H gel. As the gel changed from N–A–S–H gel to C–A–S–H gel, a significantly finer pore structure was obtained. By using the X-ray microtomography to investigate the pore structure of AAFS, similar findings were also proposed by Provis et al. [27]. The results (Figure 13) of EDS analysis was consistent with the microstructure characteristics, as shown in Figures 11 and 12. It appears that the composition of gels determined the microstructure and final engineering properties of AAFS.

4. Conclusions

In this paper, the effect of activator modulus and slag content on setting time, flowability, early age heat evolution, compressive strength, microstructure, and reaction products of alkali-activated fly ash/slag blended system were studied. Based on these studies, the following conclusions can be drawn:

(1) Both the activator modulus and slag content affected the setting time and workability of AAFS pastes. When the activator modulus was different, the effect of slag content on setting time and workability showed different trends. It indicated that a combined effect existed as the raw material and activator modulus varied.

(2) AAFS mixtures with higher slag content had a higher rate of heat release and higher extent of the reaction, leading to an increased compressive strength both at 7 d and 28 d. The increase of the activator modulus from 0 to 1.0 resulted in a higher heat release and compressive strength, while further increasing the activator modulus to 2.0 resulted in a low extent of reaction, and was unfavorable to the development of the strength. The dissolution of slag was more pronounced when NaOH was applied as the activator.

(3) The MIP results indicated that the addition of slag greatly decreased the capillary pores and increased the gel pores in AAFS, leading to lower total porosity and smaller pores. The use of Na_2SiO_3 as activator significantly refined the pores in AAFS, while further increasing the modulus from 1.0 to 2.0 resulted in a coarser pore structure.

(4) The SEM/EDS results indicated that both the activator modulus and fly ash/slag content affected the types of reaction products in AAFS. The coexistence of N–A–S–H gel and C–A–S–H gel was identified in the AAFS activated with high pH but low SiO_2 content. The C–A–S–H gel had higher space filling ability than N–A–S–H gel, resulting in a denser microstructure.

Author Contributions: Methodology and validation, Y.M.; Formal analysis, investigation and data curation, J.L.; Writing—Original draft preparation, Z.L. and X.O.; Writing—Review and editing, X.O., Y.M. and G.Y.; Supervision and project administration, Y.M.; Funding acquisition, Y.M. and X.O. All authors have read and agreed to the published version of the manuscript All authors have read and agreed to the published version of the manuscript.

Funding: This research was funded by Guangzhou Municipal Science and Technology Project (grant No. 201904010290), the Pearl River S and T Nova Program of Guangzhou (201806010188), and the Fundamental Research Funds for the Central Universities of China.

Acknowledgments: The authors are grateful for the experimental assistance from the research group of cement and concrete in South China University of Technology, China.

Conflicts of Interest: The authors declare no conflict of interest.

References

1. Bernal, S.A.; Provis, J.L. Durability of alkali-activated materials: Progress and perspectives. *J. Am. Ceram. Soc.* **2014**, *97*, 997–1008. [CrossRef]
2. Shi, C.; Qu, B.; Provis, J.L. Recent progress in low-carbon binders. *Cem. Concr. Res.* **2019**, *122*, 227–250. [CrossRef]
3. Davidovits, J. Geopolymers: Inorganic polymeric new materials. *J. Therm. Anal. Calorim.* **1991**, *37*, 1633–1656. [CrossRef]
4. Chindaprasirt, P.; De Silva, P.; Sagoe-Crentsil, K.; Hanjitsuwan, S. Effect of SiO_2 and Al_2O_3 on the setting and hardening of high calcium fly ash-based geopolymer systems. *J. Mater. Sci.* **2012**, *47*, 4876–4883. [CrossRef]
5. Ma, Y.; Ye, G.; Hu, J. Micro-mechanical properties of alkali-activated fly ash evaluated by nanoindentation. *Constr. Build. Mater.* **2017**, *147*, 407–416. [CrossRef]
6. Duxson, P.; Fernández-Jiménez, A.; Provis, J.L.; Lukey, G.C.; Palomo, A.; van Deventer, J.S. Geopolymer technology: The current state of the art. *J. Mater. Sci.* **2006**, *42*, 2917–2933. [CrossRef]
7. Hajimohammadi, A.; Ngo, T.; Vongsvivut, J. Interfacial chemistry of a fly ash geopolymer and aggregates. *J. Clean. Prod.* **2019**, *231*, 980–989. [CrossRef]
8. Hajimohammadi, A.; Ngo, T.; Kashani, A. Glass waste versus sand as aggregates: The characteristics of the evolving geopolymer binders. *J. Clean. Prod.* **2018**, *193*, 593–603. [CrossRef]

9. Lee, W.K.W.; Van Deventer, J.S.J. The effect of ionic contaminants on the early-age properties of alkali-activated fly ash-based cements. *Cem. Concr. Res.* **2002**, *32*, 577–584. [CrossRef]
10. Chindaprasirt, P.; Chareerat, T.; Sirivivatnanon, V. Workability and strength of coarse high calcium fly ash geopolymer. *Cem. Concr. Compos.* **2007**, *29*, 224–229. [CrossRef]
11. Guo, X.; Shi, H.; Dick, W.A. Compressive strength and microstructural characteristics of class C fly ash geopolymer. *Cem. Concr. Compos.* **2010**, *32*, 142–147. [CrossRef]
12. Zaharaki, D.; Komnitsas, K.; Perdikatsis, V. Use of analytical techniques for identification of inorganic polymer gel composition. *J. Mater. Sci.* **2010**, *45*, 2715–2724. [CrossRef]
13. Škvára, F.; Jílek, T.; Kopecky, L. Geopolymer materials based on fly ash. *Ceram.Silik.* **2005**, *49*, 195–204.
14. Sata, V.; Sathonsaowaphak, A.; Chindaprasirt, P. Resistance of lignite bottom ash geopolymer mortar to sulfate and sulfuric acid attack. *Cem. Concr. Compos.* **2012**, *34*, 700–708. [CrossRef]
15. Lyon, R.E.; Balaguru, P.N.; Foden, A.; Sorathia, U.; Davidovits, J.; Davidovics, M. Fire-resistant aluminosilicate composites. *Fire Mater.* **1997**, *21*, 67–73. [CrossRef]
16. García-Lodeiro, I.; Palomo, A.Y.; Fernández-Jiménez, A. Alkali–aggregate reaction in activated fly ash systems. *Cem. Concr. Res.* **2007**, *37*, 175–183. [CrossRef]
17. Gifford, P.M.; Gillott, J.E. Freeze thaw durability of activated blast furnace slag cement concrete. *ACI Mater. J.* **1996**, *93*, 242–245.
18. Soultana, A.; Valouma, A.; Bartzas, G.; Komnitsas, K. Properties of Inorganic Polymers Produced from Brick Waste and Metallurgical Slag. *Minerals* **2019**, *9*, 551. [CrossRef]
19. Lloyd, R.R.; Provis, J.L.; Smeaton, K.J.; van Deventer, J.S. Spatial distribution of pores in fly ash-based inorganic polymer gels visualised by Wood's metal intrusion. *Microporous Mesoporous Mater.* **2009**, *126*, 32–39. [CrossRef]
20. Ravikumar, D.; Neithalath, N. Effects of activator characteristics on the reaction product formation in slag binders activated using alkali silicate powder and NaOH. *Cem. Concr. Compos.* **2012**, *34*, 809–818. [CrossRef]
21. Hajimohammadi, A.; van Deventer, J.S. Dissolution behaviour of source materials for synthesis of geopolymer binders: A kinetic approach. *Int. J. Miner. Process.* **2016**, *153*, 80–86. [CrossRef]
22. Palomo, A.; Alonso, S.; Fernandez-Jiménez, A.; Sobrados, I.; Sanz, J. Alkaline activation of fly ashes: NMR study of the reaction products. *J. Am. Ceram. Soc.* **2004**, *87*, 1141–1145. [CrossRef]
23. Phoo-ngernkham, T.; Maegawa, A.; Mishima, N.; Hatanaka, S.; Chindaprasirt, P. Effects of sodium hydroxide and sodium silicate solutions on compressive and shear bond strengths of FA–GBFS geopolymer. *Constr. Build. Mater.* **2015**, *91*, 1–8. [CrossRef]
24. Criado, M.; Fernández-Jiménez, A.; De La Torre, A.; Aranda, M.; Palomo, A. An XRD study of the effect of the SiO_2/Na_2O ratio on the alkali activation of fly ash. *Cem. Concr. Res.* **2007**, *37*, 671–679. [CrossRef]
25. Somna, K.; Jaturapitakkul, C.; Kajitvichyanukul, P.; Chindaprasirt, P. NaOH-activated ground fly ash geopolymer cured at ambient temperature. *Fuel* **2011**, *90*, 2118–2124. [CrossRef]
26. Wu, X.; Jiang, W.; Roy, D.M. Early activation and properties of slag cement. *Cem. Concr. Res.* **1990**, *20*, 961–974. [CrossRef]
27. Provis, J.L.; Myers, R.J.; White, C.E.; Rose, V.; Van Deventer, J.S. X-ray microtomography shows pore structure and tortuosity in alkali-activated binders. *Cem. Concr. Res.* **2012**, *42*, 855–864. [CrossRef]
28. Ismail, I.; Bernal, S.A.; Provis, J.L.; San Nicolas, R.; Hamdan, S.; van Deventer, J.S. Modification of phase evolution in alkali-activated blast furnace slag by the incorporation of fly ash. *Cem. Concr. Compos.* **2014**, *45*, 125–135. [CrossRef]
29. ASTM. *ASTM C191-13 Standard Test Methods for Time of Setting of Hydraulic Cement by Vicat Needle*; ASTM International: West Conshohocken, PA, USA, 2013.
30. ASTM. C305 Standard Practice for Mechanical Mixing of Hydraulic Cement Pastes and Mortars of Plastic Consistency. In *Annual Book of ASTM Standards*; ASTM International: West Conshohocken, PA, USA, 2006.
31. Ma, Y.; Wang, G.; Ye, G.; Hu, J. A comparative study on the pore structure of alkali-activated fly ash evaluated by mercury intrusion porosimetry, N 2 adsorption and image analysis. *J. Mater. Sci.* **2018**, *53*, 5958–5972. [CrossRef]
32. Li, N.; Shi, C.; Zhang, Z. Understanding the roles of activators towards setting and hardening control of alkali-activated slag cement. *Compos. Part B Eng.* **2019**, *171*, 34–45. [CrossRef]
33. Ravikumar, D.; Neithalath, N. Reaction kinetics in sodium silicate powder and liquid activated slag binders evaluated using isothermal calorimetry. *Thermochim. Acta* **2012**, *546*, 32–43. [CrossRef]

34. Li, N.; Shi, C.; Zhang, Z.; Zhu, D.; Hwang, H.-J.; Zhu, Y.; Sun, T. A mixture proportioning method for the development of performance-based alkali-activated slag-based concrete. *Cem. Concr. Compos.* **2018**, *93*, 163–174. [CrossRef]
35. Provis, J.L.; Van Deventer, J.S. *Alkali Activated Materials: State-of-the-Art Report, RILEM TC 224-AAM*; Springer Science & Business Media: Berlin/Heidelberg, Germany, 2013; Volume 13.
36. Palomo, A.; Grutzeck, M.; Blanco, M. Alkali-activated fly ashes: A cement for the future. *Cem. Concr. Res.* **1999**, *29*, 1323–1329. [CrossRef]
37. Puertas, F.; Varga, C.; Alonso, M. Rheology of alkali-activated slag pastes. Effect of the nature and concentration of the activating solution. *Cem. Concr. Compos.* **2014**, *53*, 279–288. [CrossRef]
38. Ouyang, X.; Koleva, D.A.; Ye, G.; van Breugel, K. Insights into the mechanisms of nucleation and growth of C-S-H on fillers. *Mater. Struct.* **2017**, *50*, 213. [CrossRef]
39. Ouyang, X.; Koleva, D.A.; Ye, G.; van Breugel, K. Understanding the adhesion mechanisms between C–S–H and fillers. *Cem. Concr. Res.* **2017**, *100*, 275–283. [CrossRef]
40. Wang, L.; Liu, Z.; Xu, S.; Ouyang, X.; Ouyang, D.; Jiao, C.; Zhang, Y. A study on the effect of ceramic polishing powder on the nucleation and growth of hydrates in cement paste. *Crystals* **2019**, *9*, 545. [CrossRef]
41. Ouyang, X.; Pan, Z.; Qian, Z.; Ma, Y.; Ye, G.; van Breugel, K. Numerical Modelling of the Effect of Filler/Matrix Interfacial Strength on the Fracture of Cementitious Composites. *Materials* **2018**, *11*, 1362. [CrossRef]
42. Ouyang, X.; Ye, G.; van Breugel, K. Experimental and numerical evaluation of mechanical properties of interface between filler and hydration products. *Constr. Build. Mater.* **2017**, *135*, 538–549. [CrossRef]
43. Ouyang, X.; Gao, P.; Ye, G.; van Breugel, K. Effect of Filler-Hydrates Adhesion Properties on Cement Paste Strength. *ACI Mater. J.* **2018**, *115*, 437–447. [CrossRef]
44. Ouyang, X. Filler-Hydrates Adhesion Properties in Cement Paste System: Development of Sustainable Building Materials. Ph.D. Thesis, Delft University of Technology, Delft, The Netherlands, 2017.
45. Zhang, Y.M.; Sun, W.; Yan, H.D. Hydration of high-volume fly ash cement pastes. *Cem. Concr. Compos.* **2000**, *22*, 445–452. [CrossRef]
46. Ma, Y.; Yang, X.; Hu, J.; Zhang, Z.; Wang, H. Accurate determination of the "time-zero" of autogenous shrinkage in alkali-activated fly ash/slag system. *Compos. Part B Eng.* **2019**, *177*, 107367. [CrossRef]
47. Bernal, S.A. Effect of the activator dose on the compressive strength and accelerated carbonation resistance of alkali silicate-activated slag/metakaolin blended materials. *Constr. Build. Mater.* **2015**, *98*, 217–226. [CrossRef]
48. Gao, X.; Yu, Q.L.; Brouwers, H.J.H. Reaction kinetics, gel character and strength of ambient temperature cured alkali activated slag–fly ash blends. *Constr. Build. Mater.* **2015**, *80*, 105–115. [CrossRef]
49. Komnitsas, K.; Zaharaki, D.; Perdikatsis, V. Geopolymerisation of low calcium ferronickel slags. *J. Mater. Sci.* **2007**, *42*, 3073–3082. [CrossRef]
50. Komnitsas, K.; Zaharaki, D.; Perdikatsis, V. Effect of synthesis parameters on the compressive strength of low-calcium ferronickel slag inorganic polymers. *J. Hazard. Mater.* **2009**, *161*, 760–768. [CrossRef]
51. Wang, G.; Ma, Y. Drying shrinkage of alkali-activated fly ash/slag blended system. *J. Sustain. Cem. Based Mater.* **2018**, *7*, 203–213. [CrossRef]